



# Fabrication and characterization of nickel contacts for magnesium silicide based thermoelectric generators



J. de Boor<sup>a,\*</sup>, C. Gloanec<sup>a</sup>, H. Kolb<sup>a</sup>, R. Sottong<sup>a</sup>, P. Ziolkowski<sup>a</sup>, E. Müller<sup>a,b</sup>

<sup>a</sup> Institute of Materials Research, German Aerospace Center, Linder Höhe, 51147 Köln, Germany

<sup>b</sup> Institute for Inorganic and Analytical Chemistry, Justus-Liebig-Universität Gießen, Heinrich-Buff-Ring 58, 35392 Gießen, Germany

## ARTICLE INFO

### Article history:

Received 6 November 2014

Received in revised form 7 January 2015

Accepted 21 January 2015

Available online 30 January 2015

### Keywords:

Electrode materials  
Thermoelectric materials  
Sintering  
Electrical transport  
Microstructure  
Thermoelectric

## ABSTRACT

Magnesium silicide based solid solutions are highly attractive materials for thermoelectric energy harvesting due to their abundance and excellent thermoelectric properties. Identification and testing of suitable contacts is – besides material optimization – the major challenge in the development of thermoelectric modules. We have applied Ni contacts on doped Mg<sub>2</sub>Si samples using a simple one-step sintering technique. These contacts were analyzed by combining microstructural analysis with spatially resolved and temperature dependent contact resistance measurements. We observe very good adhesion, homogeneous and low contact resistances <10 μΩ cm<sup>2</sup>, as well as good stability with temperature. Three different approaches for determining the contact resistances are compared and the respective errors are discussed.

© 2015 The Authors. Published by Elsevier B.V. This is an open access article under the CC BY-NC-ND license (<http://creativecommons.org/licenses/by-nc-nd/4.0/>).

## 1. Introduction

Generators from thermoelectric materials can convert waste heat into usable electrical energy and can thus be a means to enhance the energy efficiency of various applications [1]. These generators can furthermore be used as energy source where usual electricity supply is impossible or impractical, e.g. spacecraft and mobile applications [2]. The efficiency of a thermoelectric generator is approximately proportional to the thermoelectric figure of merit  $ZT$  of the constituting thermoelectric materials.  $ZT$  itself is a combination of interdependent material properties  $ZT = \frac{\sigma S^2}{\kappa} T$ , where  $\sigma$  is the electrical conductivity,  $S$  the Seebeck coefficient,  $\kappa$  the thermal conductivity and  $T$  the absolute temperature.

Silicides and especially magnesium based silicides are very attractive materials for application in thermoelectric generators due to their excellent thermoelectric properties, their abundance, non-toxicity and low density. Employing band structure engineering, isoelectronic substitution of Si as well as nanostructuring, solid solutions from Mg<sub>2</sub>(Si, Ge, Sn) have shown  $1 < ZT < 1.5$  for several compositions [3–8].

However, for thermoelectric generators and real applications material contacting is as important as material optimization. Poor contacts can significantly degrade the module performance or even

lead to device failure [9–11]. A very simple and effective approach is the “mono bloc” or one-step sintering. In this approach powder of the thermoelectric material is compacted together with the chosen contact material in a single sintering step, e.g. in an SPS process. Due to its simplicity this process has been applied to several material classes [12,13]. For Mg<sub>2</sub>Si it has been made popular by the work of Japanese groups, who have also shown Mg<sub>2</sub>Si based thermoelectric generators [9,14–17]. Some of these works report values for contact resistances, differing however by orders of magnitude. Furthermore, all reported values are room temperature values. With target hot side temperatures for Mg<sub>2</sub>Si based generators of 400–800 K this is clearly not sufficient. Moreover, little has been revealed on the microstructure of the Mg<sub>2</sub>Si–Ni interface, which is, however, crucial for the fundamental understanding of contact formation. We have therefore combined spatially resolved contact resistance measurements to check for contact homogeneity with temperature dependent measurements of the integral contact resistance value. We have furthermore analyzed the microstructure of the contact interface and can show the formation of several different intermediate layers.

## 2. Materials and methods

Mg<sub>2</sub>Si samples with Ni electrodes were fabricated in a single sintering step similar to what is described in literature [9,16]. Polycrystalline antimony doped magnesium silicide (nominal composition Mg<sub>2</sub>Si<sub>0.9875</sub>Sb<sub>0.0125</sub>) with particle size <200 μm was used as initial source material. Further details on material fabrication

\* Corresponding author.

E-mail address: [johannes.deboor@dlr.de](mailto:johannes.deboor@dlr.de) (J. de Boor).

and compaction have been reported previously [18]. As contact material we have tested Ni foil with thicknesses of 10  $\mu\text{m}$ , 100  $\mu\text{m}$  and 300  $\mu\text{m}$ . The  $\text{Mg}_2\text{Si}$  powder and the Ni foil were stacked in a sintering form and compacted using current assisted sintering (DSP 510A, Dr. Fritsch). We have also added several boron nitride coated graphite foils between the Ni foil and the pressing stamps to facilitate easy separation of sample and pressing stamps after sintering. Sintering parameters were  $T_{\text{sinter}} = 900\text{ }^\circ\text{C}$ ,  $p = 66\text{ MPa}$  and a holding time of 10 min as we have identified these parameters as optimal parameters previously [18]. Sintering atmosphere was vacuum with  $p < 0.03\text{ mbar}$  throughout the process. For a Ni thickness of 300  $\mu\text{m}$  the fraction of cracked samples increased. This could be related to the difference in coefficient of thermal expansion between Ni and  $\text{Mg}_2\text{Si}$ . Apart from that we found no significant influence of the Ni thickness. After compaction, samples were cut for measurements. The sample used for the integral measurements had a cross section of  $A = 28.6\text{ mm}^2$ , a total thickness of 4.36 mm and a Ni foil of 100  $\mu\text{m}$  at each side. We have used a second sample with  $A = 6.92\text{ mm}^2$  and thicker Ni electrodes  $\approx 300\text{ }\mu\text{m}$  for microprobe measurements.

Spatially resolved measurements of electrical potential, contact resistances, and Seebeck coefficient were performed using a Potential-Seebeck-Microprobe (PSM) [19,20]. The setup consists of a sample stage and a moveable tip that can contact the sample at various positions. In Seebeck mode, the tip is heated and the measured temperature difference between tip and sample as well as the arising thermoelectric voltage is used to calculate the local Seebeck coefficient at the corresponding position of the sample. The Seebeck coefficient is calculated from >20 individual temperature voltage pairs. For  $\text{Mg}_2\text{Si}$  we sometimes found a noisy signal, potentially due to surface oxidation of the sample. The PSM data was therefore filtered and all points showing a standard deviation above a critical threshold (0.3%) were replaced by the mean measured value. The fraction of these filtered points was <5%. A Keithley 2700 with a switch card is used to measure temperatures and thermovoltages. In potential mode a current is driven through the sample and the tip is used to map the electrical potential at the sample surface. Both current amplitude and potential are measured using lock-in amplifiers (Femto LIA MV 150 and Stanford Research SRS830).

The tip radius is  $\approx 25\text{ }\mu\text{m}$  and the additional extension of the heated region in  $\text{Mg}_2\text{Si}$  is  $\approx 10\text{ }\mu\text{m}$ . PSM measurements were taken with a step width of 25  $\mu\text{m}$  in the direction perpendicular to the Ni- $\text{Mg}_2\text{Si}$  interface and a step width of 200  $\mu\text{m}$  in the parallel direction. Measurements of different sample sides were done consecutively after rotating the sample.

Integral measurements of electrical conductivity and contact resistances were performed in a custom-built setup described in Ref. [21]. The sample was placed between two copper blocks, contacted with a liquid metal solder and an alternating current was driven through blocks and sample, see Fig. 1. Two voltage probes were attached to the copper blocks and two further probes directly to the sample using spot welding.

The resistance that is measured at the outer probes is given by

$$R_{\text{tot}} = 2R_{\text{Cu}} + 2R_{\text{solder}} + 2R_{\text{c,met}} + 2R_{\text{Ni}} + 2R_{\text{c}} + R_{\text{Mg}_2\text{Si}}, \quad (1)$$

where we have assumed symmetry in contacts and geometry. Eq. (1) can be approximated as  $R_{\text{tot}} \approx R_{\text{Mg}_2\text{Si}} + 2R_{\text{c}}$  due to the high electrical conductivity of the copper blocks, the metal solder and the Ni electrode layer itself. Contact resistances between the copper and the solder as well as the Ni and the solder  $2R_{\text{c,met}}$  can also be neglected as these are metal-metal interfaces.  $R_{\text{Mg}_2\text{Si}}$  is the resistance of the  $\text{Mg}_2\text{Si}$  fraction of the sample and  $R_{\text{c}}$  the to be determined contact resistance. The composite electrical conductivity of the  $\text{Mg}_2\text{Si}$  sample with Ni electrodes is then given by

$$\sigma_{\text{tot}} = \frac{1}{R_{\text{tot}}} * \frac{l_{\text{Mg}_2\text{Si}}}{A}, \quad (2)$$

where  $l_{\text{Mg}_2\text{Si}}$  is the length of the sample without the Ni electrodes and  $A$  its cross section. The conductivity of the material  $\sigma_{\text{Mg}_2\text{Si}}$  can be determined directly using the voltage across the inner two voltage probes  $U_{\text{in}}$  that are positioned at distance  $l_{\text{in}}$ :

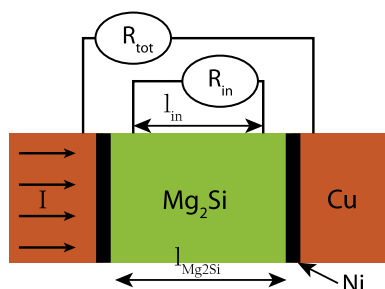


**Fig. 1.** Scheme for integral contact resistance measurements. The voltage measured across the inner probes is used to calculate the  $\text{Mg}_2\text{Si}$  material conductivity, while the voltage across the outer probes includes the contact resistances at the Ni/ $\text{Mg}_2\text{Si}$  interface.

$$\sigma_{\text{Mg}_2\text{Si}} = \frac{1}{U_{\text{in}}} * \frac{l_{\text{in}}}{A}. \quad (3)$$

The specific contact resistance  $r_{\text{c}} = R_{\text{c}} * A$  can thus be calculated using

$$r_{\text{c}} = \frac{l_{\text{Mg}_2\text{Si}}}{2} \left( \frac{1}{\sigma_{\text{tot}}} - \frac{1}{\sigma_{\text{Mg}_2\text{Si}}} \right) \quad (4)$$

For comparison we have also fabricated samples from the same powder with the same sintering parameters without Ni electrodes. In this case electrical conductivity  $\sigma_{\text{Mg}_2\text{Si,ref}}$  and Seebeck coefficient were measured in a custom-built setup [22,23] and the contact resistances were calculated using the reference data  $\sigma_{\text{Mg}_2\text{Si,ref}}$  instead of the measured  $\sigma_{\text{Mg}_2\text{Si,meas}}$ .

To investigate microstructures of the fabricated contacts SEM images were taken using a Zeiss Ultra 55 equipped with an EDX detector.

### 3. Results

A photograph of an  $\text{Mg}_2\text{Si}$  sample with Ni electrodes is presented together with an electron microscope picture of the  $\text{Mg}_2\text{Si}/\text{Ni}$  interface in Fig. 2. The photograph shows dense  $\text{Mg}_2\text{Si}$  without cracks and good adhesion between  $\text{Mg}_2\text{Si}$  and Ni.

The SEM picture confirms the good adhesion of the electrode and shows a layered interface with several distinct phases between Ni and  $\text{Mg}_2\text{Si}$ . EDX line scan and point spectrum analyses were used to identify these intermediate phases. The results of an exemplary line scan are presented in Fig. 2b), where the magnitudes of the individual intensities have been adjusted for clarity. The results of four EDX point analyses are given in Table 1.

The top and the bottom layer in the SEM picture with EDX Point 1 and 4 correspond to almost pure Ni and  $\text{Mg}_2\text{Si}$ . The region in between is a ternary mixture of Mg, Si and Ni with different ratios. An exception are the bright inclusions with a size of 1–10  $\mu\text{m}$  (e.g. at EDX point 2). These inclusions contain no or very little Mg and the composition corresponds approximately to the  $\text{Ni}_{31}\text{Si}_{12}$  phase. The phase diagram of Ni, Mg and Si exhibits various different ternary phases which might have formed at the employed sintering temperature of 900  $^\circ\text{C}$ . The composition at EDX point 3 corresponds approximately to the  $\nu$  and  $\omega$  phase [24] but a mixture

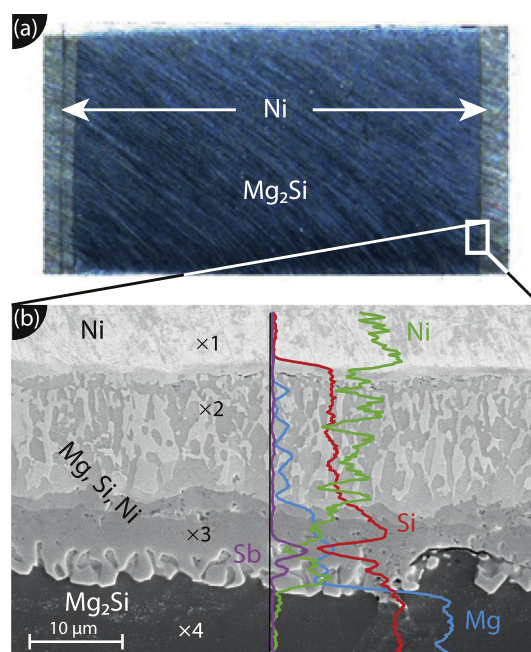


**Fig. 2.** (a) Photograph of an  $\text{Mg}_2\text{Si}$  sample with two Ni electrodes and dimensions 2.7 mm \* 2.7 mm \* 5 mm. (b): Electron microscope image of the  $\text{Mg}_2\text{Si}$  - Ni interface. The image shows several distinct layers between  $\text{Mg}_2\text{Si}$  and Ni that have formed during the sintering process. Also shown are the results of an EDX line scan and different positions ("x") where EDX elemental analyses have been performed. The results are given in Table 1.

Download English Version:

<https://daneshyari.com/en/article/7999091>

Download Persian Version:

<https://daneshyari.com/article/7999091>

[Daneshyari.com](https://daneshyari.com)